Non-perturbative Analysis of Crystals Formed by Bound Triplet States on the Shastry-Sutherland Lattice

David Schneider

Bachelorarbeit
zur Erlangung des akademischen Grades
Bachelor of Science

vorgelegt von

David Schneider

Lehrstuhl für Theoretische Physik I
Fakultät Physik
Technische Universität Dortmund
2014

Erster Gutachter: Dr. Kai Schmidt

Zweiter Gutachter: Prof. Dr. Götz S. Uhrig

Datum des Einreichens der Arbeit: 08. Juli 2014

Abstract

The bound triplet states that were recently discovered in the Shastry-Sutherland model by means of infinite projected entangled-pair states (iPEPS) are reproduced and diagonalized on open structures of different sizes. The crystals of bound states presumably responsible for the realisation of the characteristic 1/5, 1/6, 1/8 and 2/15 magnetization plateaus are composed of these super-sites using leading order graph expansions. This approach yields ground-state energies and local magnetizations which are in good agreement with iPEPS while numerically less expensive. Precise predictions of the lengths of the magnetization plateaus, however, prove to be difficult due to their high susceptibility even to small errors of the ground-state energies.

Zusammenfassung

Die kürzlich mithilfe „infinite projected entangled-pair states“ (iPEPS) entdeckten gebundenen Triplett-Zustände im Shastry-Sutherland Modell werden zunächst isoliert auf verschieden großen Strukturen reproduziert und exakt diagonalisiert. Diese Strukturen werden als Super-Plätze mithife einer Graphenentwicklung in führender Ordnung zu Kristallen zusammengesetzt, die für die Ausbildung der charakteristischen Magnetisierungsplateaus 1/5, 1/6, 1/8 und 2/15 des Shastry-Sutherland Modells im Magnetfeld verantwortlich gemacht werden. Während diese Methode im Vergleich mit iPEPS bei verringerter Rechenzeit sehr gute Übereinstimmungen in der Grundzustandsenergie sowie den lokalen Magnetisierungen liefert, gestaltet sich die Vorhersage der konkreten Länge der realisierten Plateaus aufgrund ihrer empfindlichen Abhängigkeit von der ermittelten Grundzustandsenergie als problematisch.

Contents

1. Introduction

The study of quantum spin models of highly correlated electrons is a major field in modern day solid state theory. Supported by the rapid advancement of computational physics and thus the ability to simulate systems of ever increasing sizes, substantial methodological as well as material progress has been achieved during the last decades. Whenever the magnetic coupling among particles or between particles and an external magnetic field is the dominant interaction, spin models can provide excellent means of understanding and predicting the physical properties of many experimentally accessible materials.

A fascinating class of these materials consists of frustrated quantum magnets. Frustration in this context describes the impossibility to construct a comparably simple ground state which minimizes the energy function. An example of an unfrustrated system is the well known Heisenberg model on a square lattice whose ground state is either fully polarized or Néel ordered, depending on whether the coupling is entirely ferromagnetic or antiferromagnetic, respectively. Frustration can in general be introduced either geometrically or by varying the character of the interactions, for example to a mixture of ferromagnetic and antiferromagnetic couplings. Geometrical frustration can be best understood by considering a triangular lattice with antiferromagnetic Ising coupling. The energetically optimal state of each bond is the antiparallel alignment of neighbouring spins, a state which is obviously impossible to construct even on a single triangle. As a result, frustration in general can lead to exotic ground states and new quantum phases with complex ordering (emergent phenomena) or even without any regularity at all.

A prominent example of a frustrated quantum antiferromagnet is strontium copper borate or $SrCu_2(BO_3)_2$ which is central to this thesis. Within the next paragraphs, some of the historical cornerstones in the development of the present understanding of this material and its associated spin model, the Shastry-Sutherland model, are outlined.

The chemical structure of $SrCu_2(BO_3)_2$ is shown in figure 1.1 a): it is quasi-two-dimensional and consists of alternating layers of strontium and copper borate. The compound was first synthesised by Smith and Keszler in 1991 [20] and revealed a variety of interesting properties during the following decades. Most notably, it shows a clear plateau structure in the magnetization curve [21] which could experimentally be attributed to some kind of localized magnetic superstructure [8]. Figure 1.2 shows the lower (and most controversial) part of this plateau structure.

In 1981, Shastry and Sutherland discovered an antiferromagnetic spin 1/2 Heisenberg model with a surprisingly simple ground state and an interesting sequence of quantum phases [19]. This model is introduced in detail in chapter 2; it was later

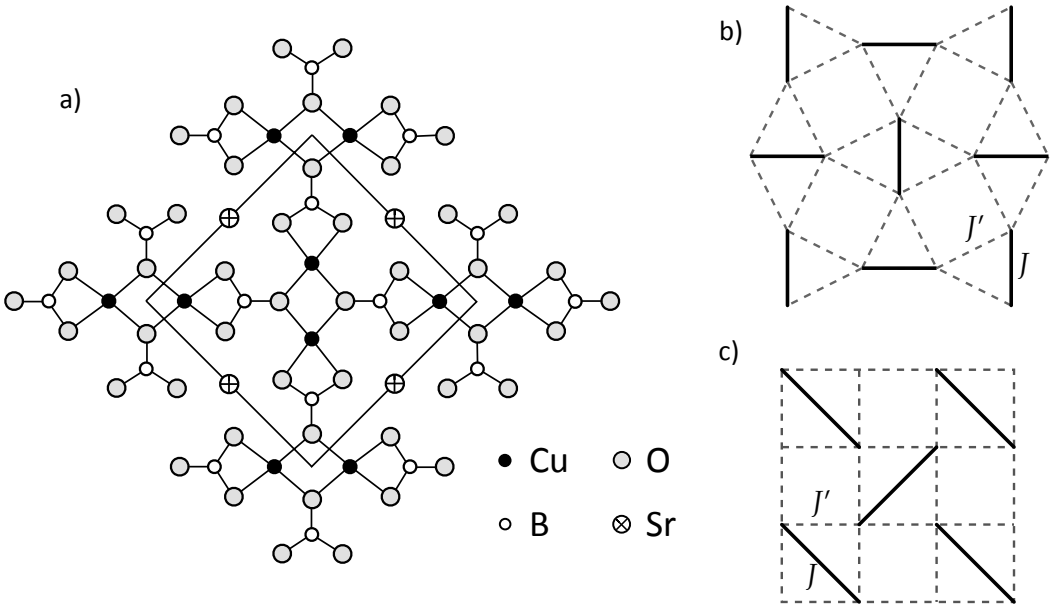

Figure 1.1.: a) Chemical structure of the quantum antiferromagnet $SrCu_2(BO_3)_2$ [8]. b) Basic structure of the Shastry-Sutherland model. The copper ions seated at the intersections of any two lines form dimers of effective spin $1/2$ particles (coupling constant J) with an additional inter-dimer coupling J'. c) Topologically equivalent illustration of the Shastry lattice, known as Archimedean snub square tiling.

discovered to be a good candidate for a theoretical description of $SrCu_2(BO_3)_2$ if each copper atom is identified with a single spin $1/2$ as illustrated in figure 1.1 b). Consequently, a lot of effort has been put into the question whether the Shastry-Sutherland model can correctly resolve the characteristic sequence of magnetization plateaus observed. Theoretical predictions of the large plateaus at $M/M_{\text{sat}} = 1/3$ and $M/M_{\text{sat}} = 1/2$ based on the assumption of a superstructure made of crystals of triplet states (see chapter 2) proved to be comparably accurate [13]. The lower plateaus, especially the plateau at $M/M_{\text{sat}} = 1/8$, however, have long eluded a satisfactory explanation [6]. Several additions to the Shastry-Sutherland model have been proposed to counter these difficulties such as the asymmetric Dzyaloshinskii-Moriya interactions or next-nearest neighbour coupling [14, 16]. Recently, a remarkably simple explanation of the lower plateaus has been given by Corboz and Mila [3]. Essentially, the prevailing conception of crystals made of single triplets needs to be dropped in favour of bound states of two triplets. While the presence of localized bound states was originally discarded by Momoi and Totsuka [15], some hints in that direction had already occured during the study of the Shastry-Sutherland model on a quasi-1d tube [7]. Figure 1.3 illustrates the difference between the two approaches; using infinite projected entangled pairs [4], Corboz and Mila showed that configuration b) is energetically favoured to configuration a). Though largely unbiased and thus allowing for unexpected discoveries, this numerical method is

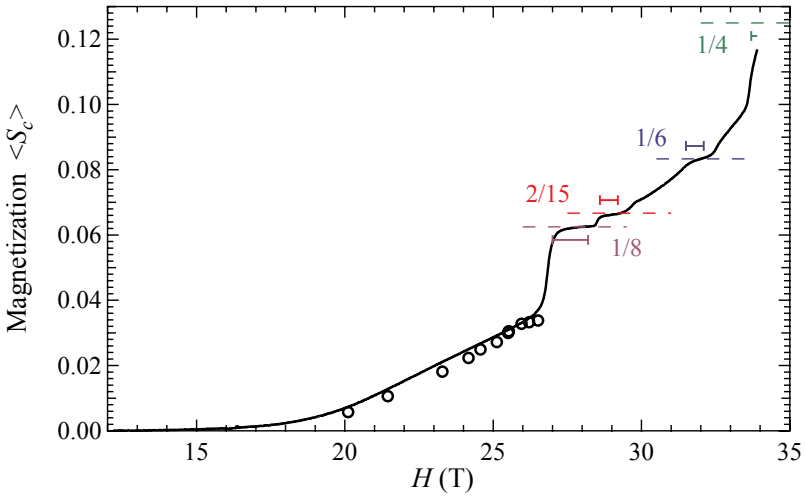

Figure 1.2.: Experimental NMR and torque measurements reveal a characteristic plateau structure in the magnetization curve of $SrCu_2(BO_3)_2$ [21].

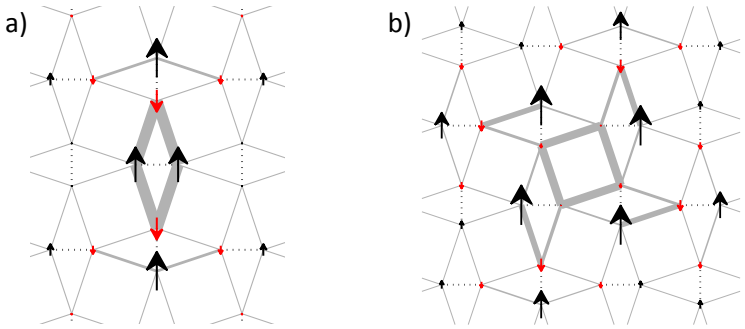

Figure 1.3.: a) Localized triplet on the Shastry-Sutherland model. The sizes of the arrows indicate the local magnetization while the thickness of a certain bond denotes its (negative) energy. b) Localized bound state of two triplets with $S^z_{\text{tot}} = 2$, visualization as in a). Both parts are taken from the work of Corboz and Mila [3].

computationally very expensive. After an overview of the most important aspects of the Shastry-Sutherland model, chapter 3 of this thesis focuses on the numerical reproduction of these bound states of triplets on finite, open clusters of moderate sizes using exact diagonalization. In chapter 4, the assembly of regular crystals from these isolated structures is presented, preceded by a motivation of the approximation techniques that are necessary in order to obtain successive estimates of their ground-state energies. Optimally, the results obtained with these techniques are good approximations of the extensive calculations performed with iPEPS and thus can serve as as a starting point for further investigation for instance of the variation of the coupling parameter J'/J.

2. The Shastry-Sutherland Model

In this chapter, some principal aspects of the Shastry-Sutherland model which are most relevant to the subsequent numerical analyses are presented. A short analytical overview of the limits of large and weak inter-dimer coupling is given as well as some details on selected parts of the phase diagram in zero magnetic field.

2.1. Basics

The Hamiltonian of the Shastry-Sutherland model in an external magnetic field h is given by

$$H = H_{\mathrm{SS}} + H_{\mathrm{field}} = J \sum_{\langle i,j \rangle} \boldsymbol{S}_i \boldsymbol{S}_j + J' \sum_{\langle\langle i,j \rangle\rangle} \boldsymbol{S}_i \boldsymbol{S}_j - h \sum_i S_i^z \tag{2.1}$$

where $\langle i,j \rangle$ denotes a dimer consisting of two sites i and j with coupling strength $J > 0$ and $\langle\langle i,j \rangle\rangle$ describes the intra-dimer interactions $J' > 0$. Basically, H_{SS} is equivalent to an antiferromagnetic Heisenberg Hamiltonian on a square lattice with an additional coupling J on every other diagonal as illustrated in figure 1.1. Using the ladder operators

$$S_i^{\pm} := S_i^x \pm \mathrm{i} S_i^y = \frac{1}{2} \left(\sigma_i^x \pm \mathrm{i} \sigma_i^y \right)$$

the dot product $\boldsymbol{S}_i \boldsymbol{S}_j$ can be written in the slightly different form

$$\boldsymbol{S}_i \boldsymbol{S}_j = S_i^z S_j^z + \frac{1}{2} \left(S_i^+ S_j^- + S_i^- S_j^+ \right) = \frac{1}{4} \left(2\pi_{ij} - \mathbb{1} \right) \tag{2.2}$$

where $\hbar$ has already been set to unity, σ are the Pauli matrices, and π_{ij} is the permutation operator of the spins i and j. From equation (2.2), it is immediately clear that $[H, S_{\mathrm{tot}}^z] = 0$ as all three summands conserve the total number of up and down spins in the system.

To obtain a first impression of the physical system described by H_{SS} it is instructive to examine the two limiting cases $J'/J \ll 1$ and $J'/J \gg 1$ first as they have both been extensively analysed and can serve as a solid starting point for further perturbative approaches [15, 12].

2.2. Limits of Large and Weak Coupling

If $J'/J \gg 1$, the intra-dimer coupling can be neglected with respect to J' and it is obvious from figure 1.1 b) that this results in a simple square lattice. The ground state

of the Heisenberg antiferromagnet on this lattice is Néel ordered, i.e. each spin is aligned antiparallel to all its neighbours, thus forming a regular pattern of alternating up and down states. Leaving out the intra-dimer coupling effectively changes the lattice geometry from triangle-based to square-based which removes the only cause of frustration. The discussion of the remaining model in an external magnetic field h remains a non-trivial task which is beyond the scope of this thesis, so only one exemplary reference is given at that point [12].

If $J'/J \ll 1$, on the other hand, H describes a number of isolated pairs of spin $1/2$ particles (dimers) so the problem can be reduced to the spectrum of

$$H_{\mathrm{D}} = J \cdot \boldsymbol{S}_1 \boldsymbol{S}_2 - h\left(S_1^z + S_2^z\right)$$

within the four-dimensional Hilbert space $\{|\uparrow\uparrow\rangle, |\uparrow\downarrow\rangle, |\downarrow\uparrow\rangle, |\downarrow\downarrow\rangle\}$. The eigenstates of a system of $N/2$ dimers can then be expressed as product states of the eigenvectors of H_{D}

$$|\psi\rangle = \prod_{i=1}^{N/2} |\phi_i\rangle \quad \text{with} \quad |\phi_i\rangle \in \mathrm{Eig}\, H_{\mathrm{D}},$$

and the corresponding eigenvalues are obtained by simple summation. For $h = 0$, this is basically the angular momentum coupling of two spin $1/2$ particles, so the eigenstates of H_{D} can be easily constructed using the Clebsch-Gordan coefficients:

$$|s^0\rangle := \frac{1}{\sqrt{2}}\left(|\uparrow\downarrow\rangle - |\downarrow\uparrow\rangle\right) \qquad |t^0\rangle := \frac{1}{\sqrt{2}}\left(|\uparrow\downarrow\rangle + |\downarrow\uparrow\rangle\right)$$
$$|t^-\rangle := |\downarrow\downarrow\rangle \qquad |t^+\rangle := |\uparrow\uparrow\rangle$$

The first eigenstate is the singlet state $|s^0\rangle$ with the corresponding energy $E = -3/4J$, the other three states form a triplet with the energy $1/4J$. The superscripts "+", "0" and "−" denote the local magnetization of the state, i.e. the eigenvalue of $S_1^z + S_2^z$ which is either 1, 0 or -1.

This analogy between a triplet state and a spin 1 particle leads to the possible interpretation of the triplet state as the presence (and, correspondingly, the singlet state as the absence) of a bosonic quasi-particle. Though rather technical in the limit $J' \to 0$, this observation proves to be very useful for the examination of the more interesting cases with finite inter-dimer coupling. For certain values of J'/J, this analysis is further simplified by the fact that the singlet product state remains the exact ground state of H (see next section). For $J' \neq 0$, the number of these triplets is no longer conserved. It is, however, possible to derive an effective Hamiltonian which conserves the number of so-called "dressed triplets" or "triplons" [18] which hop and interact by virtual triplets in a number of different ways [15]. Since a detailed deduction of the effective model of the Shastry-Sutherland model is beyond the scope of this thesis, we only summarize its strong-coupling expansion up to order two in J'/J in appendix A.1.

So far, the influence of the magnetic field has not been discussed. Because of the

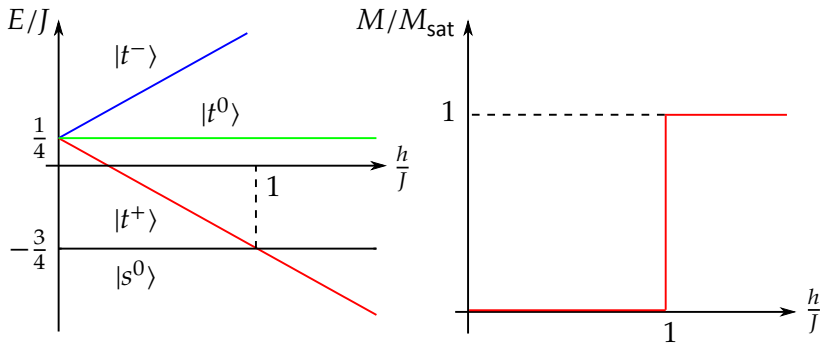

Figure 2.1.: Spectrum and magnetization of a single dimer with coupling strength J at $T = 0$. If $h > J$, the $|t^+\rangle$ triplet state is energetically lower than the singlet state due to Zeeman splitting and both spins are aligned parallel to the external field. This leads to a discontinuity in the magnetization.

conservation of S^z_{tot}, the eigenstates deduced above remain eigenstates independent of h while their energy can be simply expressed by

$$E(h) = \langle H(h) \rangle = E(0) - h \langle S^z_{\text{tot}} \rangle . \tag{2.3}$$

Note that equation (2.3) still holds true in the general case where J and J' are non-zero and thus can be used to decompose the analysis of the Shastry-Sutherland model in an external magnetic field into the determination of $E(0)$ and the local magnetization of the corresponding eigenstate. In the dimer case $J' = 0$, equation (2.3) describes a Zeeman splitting of the previously degenerate triplet states which is illustrated in the left part of figure 2.1.

If we assume zero temperature, the system always resides in its ground state, so there is a critical value of the magnetic field h_{crit} for which the energy of the $|t^+\rangle$ triplet state crosses the energy of the previous singlet ground state. This leads to the magnetization curve depicted in the right part of figure 2.1 which is discontinuous at $h = h_{\text{crit}} = J$. So for $J' = 0$ there is a first order phase transition at $h = h_{\text{crit}}$ from the non-magnetic singlet phase to the magnetic triplet phase.

If the coupling J' is neither negligible nor dominant, the magnetization curve shows a complex sequence of plateaus at several fractions of the saturation value, connected by a variety of in-between phases which cannot be presented in detail at this point. Instead, we focus on the phase transitions induced by variation of J'/J in the next short section and come back to the magnetization plateaus in chapter 4.

2.3. Phase Diagram in Zero Field

As can be seen in figure 1.1 b), the Shastry-Sutherland bonds form a regular pattern of equilateral triangles whose base always consists of an intra-dimer bond while its other sides are inter-dimer couplings. Thus the elements of the second sum in

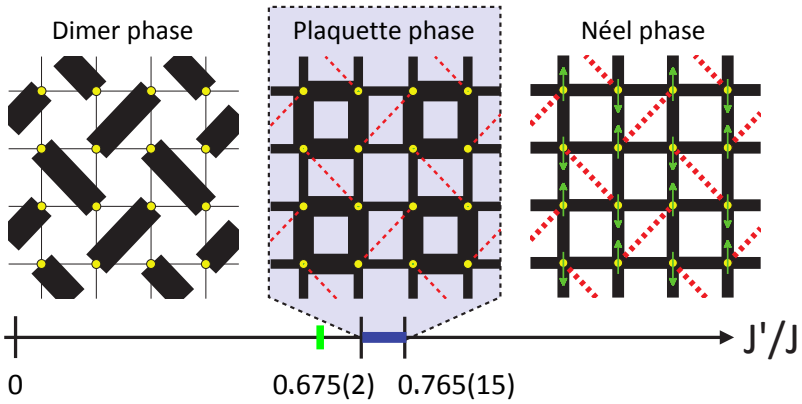

Figure 2.2.: Phase diagram of the Shastry-Sutherland model obtained with iPEPS [4]. The thickness of a line represents the energy of the corresponding bond, solid (dashed) lines denote a negative (positive) sign. The green dash on the J'/J-axis marks the assumed coupling constant of $SrCu_2(BO_3)_2$.

equation (2.1) can be rearranged in a very natural way:

$$J' \sum_{\langle\langle i,j\rangle\rangle} \boldsymbol{S}_i \boldsymbol{S}_j = J' \sum_{\triangleright(i,j,k)} \left(\boldsymbol{S}_i + \boldsymbol{S}_j\right) \boldsymbol{S}_k \tag{2.4}$$

The notation $\triangleright(i,j,k)$ implies that the sites i and j belong to the same dimer, so they are coupled via J, while k belongs to one of the neighbouring dimers and is coupled to both i and j via J'. Recalling the fact that a product state of singlets is an exact eigenstate of H_{SS} for $J' = 0$, a close look at equation (2.4) reveals that this is also true for arbitrary values of J' as the total spin $\boldsymbol{S}_i + \boldsymbol{S}_j$ vanishes for any singlet $\langle i,j\rangle$. This is a direct consequence of the geometric frustration caused by the triangular structure of the lattice.

Even more astonishing is the fact that this product state remains the exact ground state for $J'/J \in [0, 0.68]$ [4]. A value of $J'/J \approx 0.63$ seems to match the experimental data of $SrCu_2(BO_3)_2$ best [13], so the substance is still within this dimer phase; this value is used in all calculations unless otherwise noted. For $J'/J > 0.77$ the ground state is Néel ordered as discussed in the limit of high inter-dimer coupling above. The range in between has been subject to several speculations; recent calculations, however, show a clear tendency towards a plaquette phase with long-range order where four sites form a singlet [11, 4]. Figure 2.2, which summarizes the complete phase diagram as it is known to date, concludes the discussion of the Shastry-Sutherland model. In the next chapter, this model is solved numerically on several clusters of different sizes and symmetries.

3. Isolated Bound States of Triplets

The aim of this chapter is to investigate the constituents of the crystals discovered by Corboz and Mila [3]. As these are bound states of two triplets t^+, this is done by solving the Shastry-Sutherland model on finite clusters for $S^z_{\text{tot}} = 2$ using exact diagonalization techniques. The abilities and limitations of these techniques are presented in the first sections, followed by a detailed discussion of the results.

3.1. Methodological Background

One of the numerical techniques to be applied extensively in this work is exact diagonalization (ED). This section is dedicated to its physical motivation as well as its mathematical realisation using the Lanczos algorithm. The most important approaches to reduce memory consumption are presented and discussed in some technical detail.

3.1.1. Exact Diagonalization

Once a model Hamiltonian H has been found for a particular solid, further non-relativistic analysis usually involves at some some point the solution of the time-independent Schrödinger equation

$$H|\psi\rangle = E|\psi\rangle\,. \tag{3.1}$$

If the Hilbert space $\mathcal{H}$ of the problem can be chosen to be finite-dimensional, for example by using certain symmetries or, as in this work, by applying open boundary conditions, equation (3.1) can be mapped to an n-dimensional eigenvalue problem by choosing an arbitrary basis of $\mathcal{H}$ and representing H in terms of that basis. The dimension n of this matrix representation depends on the relevant properties of the particles modelled by H; if N static particles with spin S and no other degrees of freedom are considered, it is simply given by $n = (2S+1)^N$.

If $S = 1/2$, as in the Shastry-Sutherland model, $N = 32$ leads to a matrix with approximately $1.8 \cdot 10^{19}$ entries which is impossible to store even on a supercomputer, so it is not feasible to use any eigensolver involving the parallel manipulation of the entire matrix such as the Jacobi transformation method. As many simulations are performed at or close to zero temperature where the system is assumed to be in (or energetically close to) its ground state, a few of the lowest eigenvalues of H already contain much of the relevant physical information. There are basically two families

of algorithms specifically designed for this purpose, the Lanczos algorithm [9] and the Davidson algorithm [5], the former being discussed in the next section.

3.1.2. Lanczos Algorithm

In this section, the mathematical background of the Lanczos algorithm is summarized; the implementational details are presented in appendix A.2. For a more thorough introduction to the practical application of Krylov subspace methods, see for example the textbook by Parlett [17].

The basic procedure suggested by Lanczos obtains an approximation of the lowest eigenvalue and eigenvector of a real symmetric or complex Hermitian matrix A [9]. This is done by creating a random starting vector $\boldsymbol{v}$ and successively building an orthonormal basis of its Krylov space

$$\mathcal{K}_j(\boldsymbol{v}) := \text{span}\,\{\boldsymbol{v}, A\boldsymbol{v}, A^2\boldsymbol{v}, \dots, A^{j-1}\boldsymbol{v}\}$$

in each step j using Gram-Schmidt orthogonalization. It can be shown that for all j the projection of A to $\mathcal{K}_j$ is a tridiagonal matrix T_j with respect to that basis, finally resulting in

$$A = UT_nU^*$$

where U denotes some invertible matrix. There are two advantages of building a basis in this rather complicated way. First, orthogonalization has only to be performed against the two preceding vectors in each step as all the other scalar products appearing in the Gram-Schmidt process vanish. Second, the expansion from $\mathcal{K}_j$ to $\mathcal{K}_{j+1}$ causes the largest (smallest) eigenvalue of T_j to increase (decrease) monotonously as the gradients of their corresponding Rayleigh quotients are successively included in each step. Because of $\mathcal{K}_i \subset \mathcal{K}_{i+1} \subset \mathbb{R}^n$ or $\mathbb{C}^n$, they are at the same time bounded above (below) by the largest (smallest) eigenvalue of A. In practice, this leads to a rapid convergence of the extremal eigenvalues of T_j to the extremal eigenvalues of A, so the algorithm can be aborted after a number of steps which is in general small compared to the dimension n of the matrix A. The norm of the residual $\boldsymbol{r}^{(j)}$ of the eigenvector after j steps is easily accessible using

$$\left\|\boldsymbol{r}^{(j)}\right\| = \left|\beta_j s_j^{(j)}\right|$$

and can thus be used as a criterion for convergence. Here, $s_j^{(j)}$ denotes the last component of the normalized eigenvector of T_j corresponding to λ_j. Depending on the length of the vectors, the residual of the lowest eigenvalue can be several orders of magnitude smaller than $\left\|\boldsymbol{r}^{(j)}\right\|$, so the choice of the tolerance ϵ requires some care.

Once the lowest eigenvalue has converged, some technical difficulties may arise from the fact that numerical calculations are usually performed using finite precision. Accumulated rounding errors slowly lead to a loss of orthogonality in the Krylov basis until the vectors $v_1, \dots v_k$ finally are linearly dependent. To counteract this process, several improvements can be applied to the basic Lanczos scheme.

Their implementation is essential when the algorithm is used to compute more than one eigenvalue or when convergence is expected to be slow, for example when the lowest eigenvalues are very close to each other. The cases encountered during this work, however, are unproblematic as convergence can usually be achieved after less than 150 iterations with $\epsilon = 10^{-9}$. It should also be noted that the basic Lanczos algorithm cannot correctly resolve degeneracies due to the appearance of so-called spurious eigenvalues or ghosts once the ground state has converged and orthogonality is lost.

One further advantage of the simple Lanczos algorithm is the (exclusive) evaluation of A in a single matrix-vector product which can take advantage of any storage scheme or even be performed "on-the-fly" when all memory is used to store the Lanczos vectors. In the latter case, the minimal memory requirement for the determination of the ground-state energy is roughly $24n$ bytes as the three vectors $\boldsymbol{v}_i, \boldsymbol{v}_{i+1}$ and $\boldsymbol{r}$ of double precision and length n have to be kept in memory simultaneously. To calculate the corresponding approximation of the eigenvector of A, the algorithm either has to be restarted using the same starting vector $\boldsymbol{v}_0$ or all $\boldsymbol{v}_i$ have to be written to disk. In any case, another $8n$ bytes are required to store the resulting eigenvector. In the special case that A is the representation of the Shastry-Sutherland Hamiltonian H_{SS}, it is helpful to use the conservation of S^z_{tot} so the N-particle Hilbert space $\mathcal{H}$ can be written as the direct sum

$$\mathcal{H} = \mathcal{H}_{-\frac{N}{2}} \oplus \mathcal{H}_{-\frac{N}{2}+1} \oplus \cdots \oplus \mathcal{H}_{\frac{N}{2}-1} \oplus \mathcal{H}_{\frac{N}{2}}$$

where

$$\langle\psi|S^z_{\mathrm{tot}}|\psi\rangle = x \quad \forall\, |\psi\rangle \in \mathcal{H}_x.$$

By choosing an appropriate basis E, the matrix representation of H_{SS} is block diagonal, so the problem can be decomposed into the diagonalization of $N+1$ smaller matrices. The obvious choice for a number of spin 1/2 particles is

$$E = \prod_{i=1}^{N} \{|\uparrow\rangle, |\downarrow\rangle\} = \bigcup_{x=-\frac{N}{2}}^{\frac{N}{2}} E_x$$

with

$$\begin{aligned} E_x &:= \{|\psi\rangle \in E : \langle\psi|S^z_{\mathrm{tot}}|\psi\rangle = x\} \\ &= \{|\psi\rangle \in E : \mathrm{Ham}\,(\mathrm{Int}\,|\psi\rangle) - N/2 = x\}. \end{aligned}$$

The function Ham returns the Hamming weight, i.e. the number of ones in the binary representation of Int $|\psi\rangle$ which is given by

$$\mathrm{Int}\,|\psi\rangle := \sum_{i=0}^{N-1} \left(\langle\downarrow|^{\otimes i} \otimes \langle\uparrow| \otimes \langle\downarrow|^{\otimes N-1-i}\right) |\psi\rangle\, 2^i. \tag{3.2}$$

While the decomposition of $\mathcal{H}$ into its subspaces with constant S^z_{tot} greatly reduces memory consumption, this approach also entails new challenges concerning the storage and administration of the basis states. The integer representations of the elements of E as defined by equation (3.2) are $0, 1, \ldots, 2^N - 1$. Their binary representations obviously have a length of N bits, each one representing the spin quantum number of a certain particle, being either set (spin-up state) or unset (spin-down state). Furthermore, the basis states can naturally be numbered by their integer representation. The elements of E_x with constant S_z, however, are represented by a set of integers with constant Hamming weight. In order to calculate the necessary matrix elements, these states also have to be counted in some way, i.e. a bijective function

$$f : \{x \in \mathbb{N} \cap [0, 2^N - 1] : \text{Ham}\,(x) = c\} \rightarrow \left\{1, 2, \ldots, \binom{N}{c}\right\} \tag{3.3}$$

is needed. Otherwise, a search would have to be performed each time H_{SS} acts on a basis state. As the matrix vector operation is by far the most CPU dominating part of the Lanczos algorithm, this is usually not desirable. Fortunately, there is a very convenient way to construct such a mapping, known as Lin Coding [10], which will be presented in the next section.

3.1.3. Lin Tables

The naive way of implementing a mapping f as described in (3.3) might be to use a vector of length 2^N which is indexed using the integer representations and contains the numbering of the respective basis states. While certainly optimal in terms of access time, this approach typically wastes between 75% and 99% (depending on N and S^z_{tot}) of memory which could have been used to store the Lanczos vectors instead. This is because only those basis states that are actually contained in the E_x under consideration will ever be looked up, so a fraction of memory of

$$u = \frac{1}{2^N}\binom{N}{\frac{N}{2} + S^z_{tot}}$$

remains unused throughout the calculation. Employing hashing techniques drastically reduces the problem, but for large N the number of collisions caused by the usual hashing functions involving the modulus operation also increases considerably.

The idea proposed by Lin is to create a two dimensional search space instead of the one dimensional list of states. Using his notation, let I denote the integer representation and J the number of the state to be looked up. If N is assumed to be even for the sake of simplicity, the binary representation of I can be split into two parts of equal length, I_a and I_b. A set of vectors J_a and J_b is introduced such that

$$J(I) = J_a(I_a) + J_b(I_b), \tag{3.4}$$

where J_a is called the support vector and J_b the directional vector in analogy to analytic geometry. While the naive implementation of J mentioned above comprised 2^N integers, the two vectors associated with J_a and J_b combined have at most $2 \cdot 2^{N/2}$ entries. For $N = 32$ and $S^z_{\text{tot}} = 2$ this saves about 99.997% of memory. The vectors J_a and J_b can easily be chosen in a way such that the mapping (3.4) is unique by using alternate assignment; the detailed procedure can be found in appendix A.2. Any lookup now only involves one evaluation of (3.4) which can be done very efficiently.

This approach can in principle be extended using a three- or even higher-dimensional lookup field, but further savings of resources usually do not justify the additional implementational effort. The reverse lookup procedure, i.e. obtaining the integer representation of state i, obviously requires the storage of the integer representations of all states, sorted according to their numbering. The size of that field usually becomes the limiting factor long before an extension of the lookup field seems advisable.

Using the techniques described in the previous sections, it is possible to analyse the $S^z_{\text{tot}} = 2$ subspace of an open Shastry-Sutherland cluster consisting of up to 16 dimers ($N = 32$) on a machine with 25 GB of main memory available.

3.2. Results: Pinwheel Structures

In this section, the results obtained by ED on five different clusters are presented. As mentioned above, the analysis is restricted to the $S^z_{\text{tot}} = 2$ subspace where a single bound state of two triplets is expected to be found. The local magnetizations as well as the singlet / triplet densities are extracted from the eigenvectors and the symmetry of the corresponding wave function is analysed.

The upper part of figure 3.1 shows four C_4-symmetric structures consisting of 8, 12 and 16 dimers, respectively. Additionally, a less symmetric cluster of 14 dimers is analysed as can be seen in figure 3.2. The respective ground-state energies are listed in table 3.1.

Number of dimers	Symmetry	E_0/N
8	C_4	−0.310 40
12	C_4	−0.334 44
14	C_2	−0.342 27
16	C_4	−0.347 75

Table 3.1.: Ground state energies per site of the five different structures obtained with ED.

If $\{|b_i\rangle\}$ denotes the natural product basis E_2 of that subspace as introduced in the previous section, the eigenvector is available in the form

$$|0\rangle = \sum_{|b_i\rangle \in E_2} c_i \, |b_i\rangle \, .$$

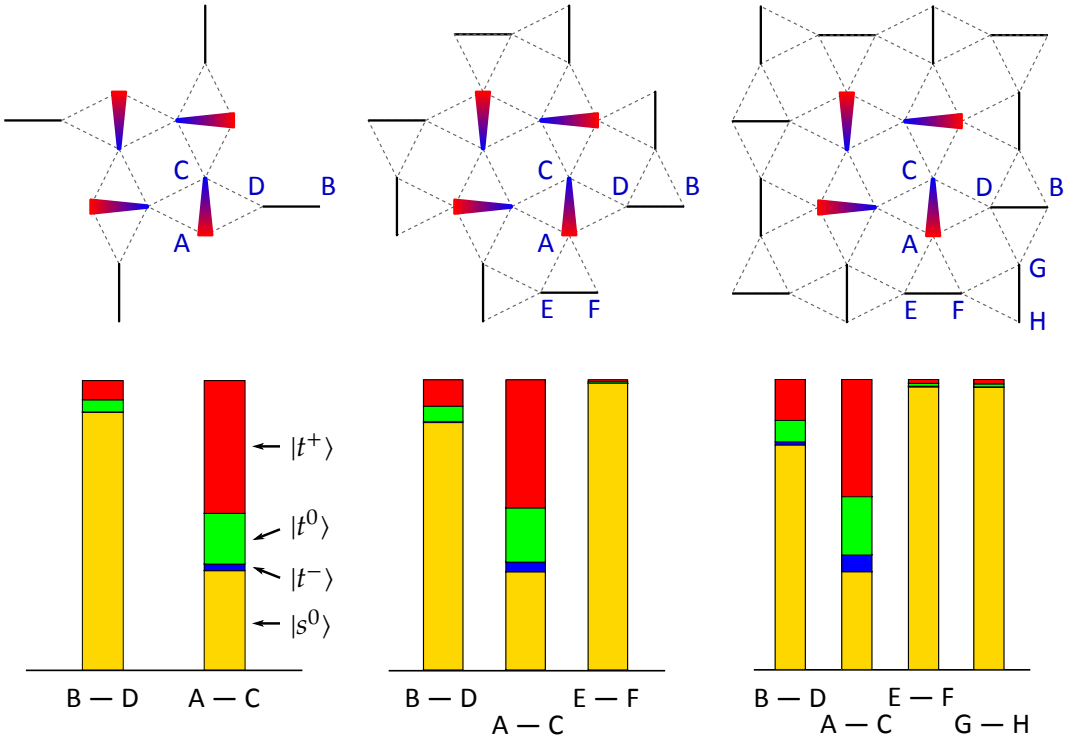

A	0.41783
B	0.18849
C	0.01764
D	−0.12396

A	0.40116
B	0.21190
C	0.00680
D	−0.12537
E	−0.03728
F	0.04279

A	0.36292
B	0.24313
C	−0.01667
D	−0.11310
E	−0.04517
F	0.05555
G	−0.04769
H	0.06104

Figure 3.1.: Graphical representation of the results obtained with ED on four symmetric structures. For each cluster, the local magnetizations are given in tabular form as well as the distribution of the singlet / triplet densities. Symmetrically equivalent sites are only listed and labelled once.

A	B	C	D	E	F	G	H
0.3496	0.2347	−0.035 74	−0.091 54	−0.053 57	0.0625	−0.054 27	0.074 75
0.3491	0.2453	−0.005 462	−0.1081	−0.058 10	0.069 71	−0.054 44	0.074 70
0.3515	0.2343	−0.036 06	−0.092 74	−0.053 19	0.0619	−0.053 53	0.073 91
0.3509	0.2461	−0.005 571	−0.1087	−0.057 55	0.069 46	−0.054 36	0.074 54

Table 3.2.: Local magnetizations on a cluster of 16 dimers obtained with iPEPS [2]. As the variational results are not perfectly symmetric, four numbers are listed for each of the designated sites in clockwise order.

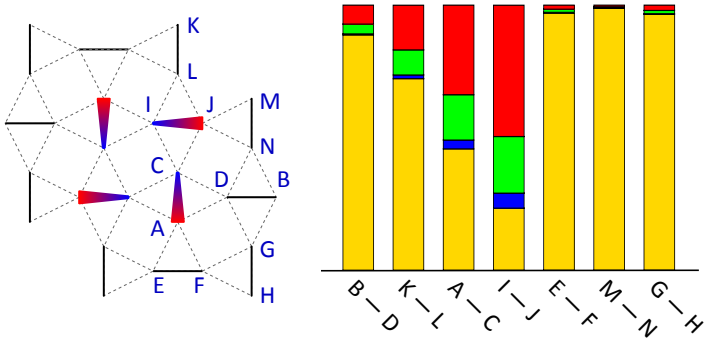

A	0.37279	J	0.39146
B	0.16694	K	0.28462
C	−0.06831	I	−0.04710
D	−0.09926	L	−0.12976
E	−0.06152	N	−0.02038
F	0.07374	M	0.02518
G	−0.05637		
H	0.07378		

Figure 3.2.: Graphical representation of the results obtained with ED on a C_2-symmetric cluster of 12 dimers. Illustrations as in figure 3.1.

To calculate the relevant observables, we define two auxiliary operators. First, the rotation operator

$$R(\theta) : \mathcal{H} \to \mathcal{H}$$

rotates the N sites of a C_4-symmetric structure by an angle of θ, this is achieved practically by a sequence of permutations. By numerical verification of

$$\langle 0|R(\pi/2)|0\rangle = \langle 0|R(\pi)|0\rangle = 1,$$

on the smallest cluster, the ground state is found to have s-wave symmetry. Second, the single site projection operator

$$P(|\psi\rangle_i) : \mathcal{H} \to \mathcal{U} \qquad |\psi\rangle_i \in \text{span}\ \{|\uparrow\rangle, |\downarrow\rangle\}$$

projects a state onto the subspace

$$\mathcal{U} = \prod_{k=1}^{i-1} \{|\uparrow\rangle, |\downarrow\rangle\} \otimes \text{span}\ |\psi\rangle \otimes \prod_{k=i+1}^{N} \{|\uparrow\rangle, |\downarrow\rangle\}$$

and thus can be written as

$$P(|\psi\rangle_i) = \mathbb{1}^{\otimes i-1} \otimes |\psi\rangle\langle\psi| \otimes \mathbb{1}^{\otimes N-i-1}. \tag{3.5}$$

If $\mathcal{H}$ is decomposed into a product of dimer spaces $\mathcal{D}_i$, a dimer projection operator

$$D(|\psi\rangle_i) : \mathcal{H} \to \mathcal{V} \qquad |\psi\rangle_i \in \text{span}\ \{|\uparrow\uparrow\rangle, |\uparrow\downarrow\rangle, |\downarrow\uparrow\rangle, |\downarrow\downarrow\rangle\} = \mathcal{D}_i$$

onto the subspace

$$\mathcal{V} = \prod_{k=1}^{i-1} \mathcal{D}_k \otimes \text{span}\ |\psi\rangle \otimes \prod_{k=i+1}^{N/2} \mathcal{D}_k$$

can be defined in exactly the same way with the only replacement $N \to N/2$ in equa-

tion (3.5). The local magnetization of site k can now easily be calculated using

$$\langle S_k^z \rangle = \frac{1}{2} \sum_{|b_i\rangle \in E_2} |c_i|^2 \left[\langle b_i | P \left(|\uparrow\rangle_k \right) |b_i\rangle - \langle b_i | P \left(|\downarrow\rangle_k \right) |b_i\rangle \right].$$

The singlet density $\rho_{|s^0\rangle_k}$ as well as the three different triplet densities $\rho_{|t^*\rangle_k}$ are defined as

$$\begin{aligned} \rho_{|s^0\rangle_k} &:= \langle 0 | D \left(|s^0\rangle_k \right) |0\rangle \\ \rho_{|t^*\rangle_k} &:= \langle 0 | D \left(|t^*\rangle_k \right) |0\rangle . \end{aligned} \tag{3.6}$$

For practical computation in the given basis E_2, it is more convenient to write for a given k and for all i

$$c_i |b_i\rangle = c_i^{|d_i\rangle} |a_i d_i e_i\rangle \quad \text{where} \quad |d_i\rangle \in \mathcal{D}_k.$$

so equation (3.6) becomes e.g. for the singlet density

$$\rho_{|s^0\rangle_k} = \frac{1}{2} \sum_{\substack{a_i, e_i \\ |a_i \uparrow \downarrow e_i\rangle \in E_2}} \left| c_i^{|\uparrow\downarrow\rangle} - c_i^{|\downarrow\uparrow\rangle} \right|^2 .$$

Using similar projector algebra, the correlation functions of any two dimers can also be obtained which may be of interest for future perturbative calculations. The relevant relations are compiled in appendix A.3 as they do not add any substance to the current analysis.

The results of these calculations are illustrated in the histograms of figures 3.1 and 3.2. Figure 3.3 shows the evolution of a bound state in the $S^z_{\text{tot}} = 2$ channel of the cluster consisting of 12 dimers as a function of the coupling strength J'/J.

It is observed that the ground-state energy per site decreases monotonically with an increasing number of dimers. This is probably a consequence of the increasing delocalization of the bound state which can also be observed in the asymmetric cluster (figure 3.2) when comparing the triplet densities on the two symmetry axes which consist of 4 and 2 dimers, respectively.

If the local magnetizations of the structure of 16 dimers are compared to the values obtained with iPEPS as presented in table 3.2 and figure 1.3 b), the ED calculations are in good agreement with the variational results. Note that for the ED calculations a certain symmetry has been introduced by choice of the different clusters while the variational ansatz uses no such assumptions and thus does not produce perfectly symmetric results. As the figures in table 3.2 have been obtained with a finite "entanglement parameter" $D = 10$, there is no significant disagreement between iPEPS and ED at this point.

The density histograms show that the outer dimers of the medium and large clusters have a probability approaching one of being in a singlet state. Considering equation (2.4), this justifies the assumption that the groundstate of such a system is not going to change significantly when additional couplings J' are introduced at the border line. This observation motivates the following chapter where regular crys-

tals of bound states are assembled using a combination of the structures presented in figures 3.1 and 3.2 as a starting point.

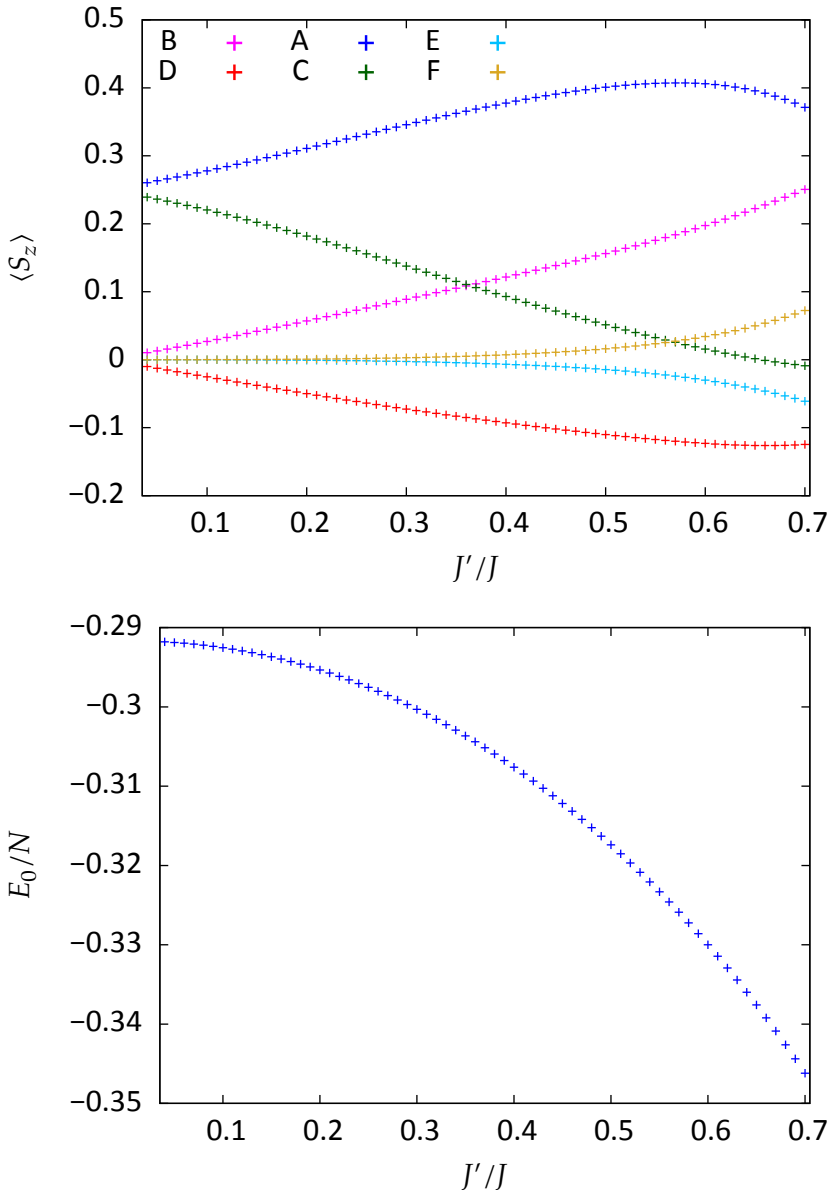

Figure 3.3.: Local magnetizations (top) and ground-state energy per site (bottom) on a cluster of 12 dimers as a function of the inter-dimer coupling ratio J'/J. The positions of the sites A to F are shown in figure 3.1.

4. Crystals of Bound States

4.1. Assembly of the Crystals

After the analysis of isolated bound state of triplets, the next step in the reproduction of the results obtained by Corboz and Mila [3] is the assembly of crystals of these bound states. Their work is used as a guideline on how the unit cells of these crystals should be constructed in the case of the 1/6, 1/5, 1/8 and 2/15 plateaus. Using different combinations of the five structures analysed with ED, a regular pattern covering the entire lattice is developed for each of the fractional magnetizations as can be seen in figures 4.1 and 4.2. Once an estimate of the ground state of the large system without an external field has been calculated, equation (2.3) can be used to obtain the energy as a function of the external magnetic field h. As the system is always supposed to reside in the energetically lowest state, it is possible to predict which of a set of plateaus is realized for a given h.

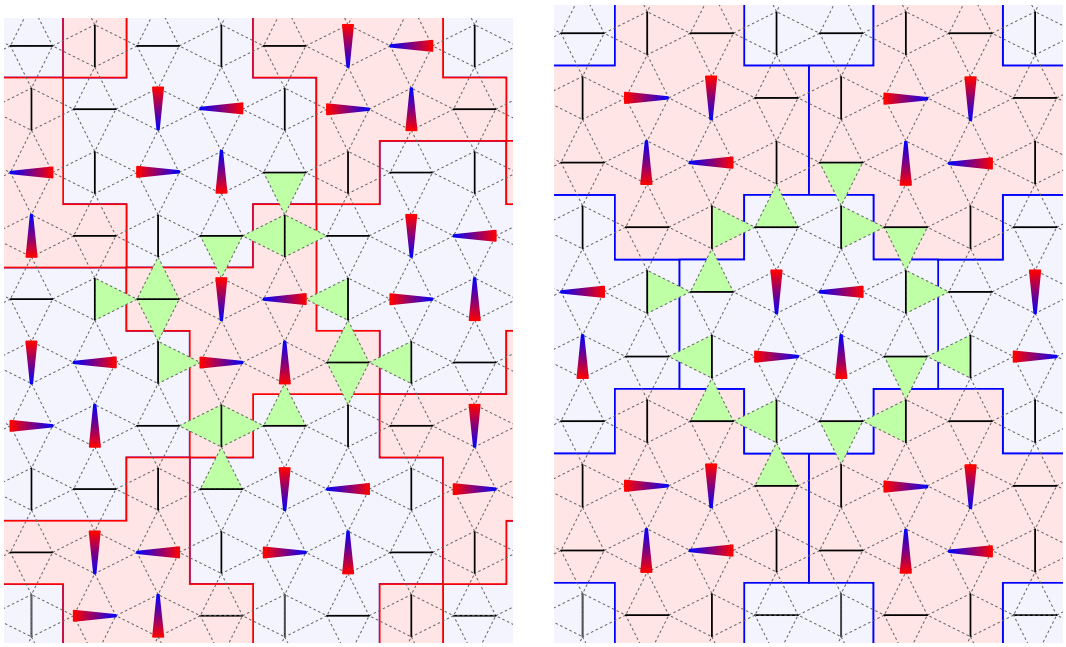

Figure 4.1.: *Left:* Crystal "1/5", composed of alternating clusters of 8 and 12 dimers. *Right:* Crystal "1/6 rectangular", composed of alternating stripes of original and mirrored clusters of 12 dimers. *Both:* The corrections to the energy of the unit cell caused by the green Shastry bonds connecting two clusters are weighted by 1/2.

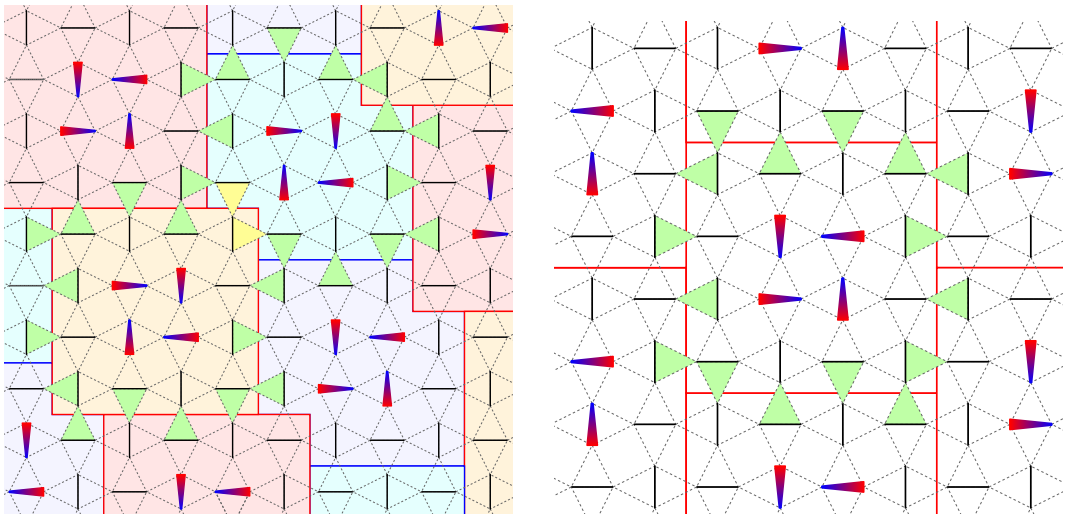

Figure 4.2.: *Left:* Crystal structure "2/15", composed of alternating stripes of original and mirrored clusters of 12 and 14 dimers. The corrections to the energy of the unit cell caused by the yellow Shastry bonds connecting two clusters within the unit cell are weighted fully.
Right: Crystal structure "1/8 rhomboid", composed of clusters of 16 dimers.

The next sections are basically concerned with the determination of these ground-state energies using several approximation techniques, starting from the simple product state of the isolated wave functions. Two of these techniques, namely graph expansion and (selective) truncation of the Hilbert space, are presented in the following two sections.

4.2. Methodology

4.2.1. Graph Expansion

The basic idea of a graph expansion or linked cluster expansion is the decomposition of the ground-state energy of a finite or an infinite lattice into a number of contributions associated with a connected graph of a certain topology. In the spirit of an effective model describing quasi-particles, these contributions can be interpreted as fluctuations between the nodes of such a graph, so all fluctuations contained within a certain graph G are also contained in every graph that contains G. As a result, care has to be taken in order not to count a certain contribution multiple times. This can be achieved by subtracting the contributions of all subgraphs from the energy of the graph under consideration; the remaining value is the energy associated with fluctuations specific to that graph. The important question is whether these contributions decrease with an increase in the length of the graph, so the expansion can be truncated at some point.

If the structures analysed in the previous chapter are arranged on the Shastry-

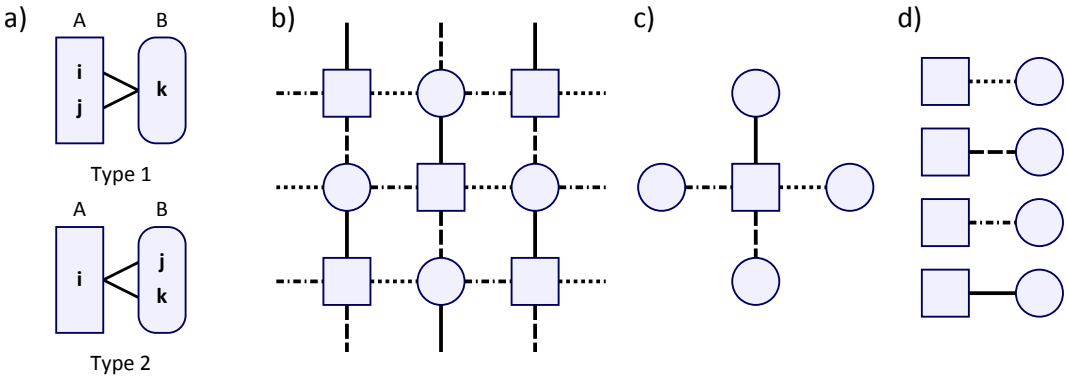

Figure 4.3.: a) Two types of interactions crossing the border line between the pinwheel structures A und B. The coupling parameter always is J'.
b) to d) First order graph expansion on a periodic lattice with two kinds of super-sites, denoted by a circle and a square, and four kinds of super-bonds, illustrated by different line styles. Part b) shows the complete lattice which is reduced to an expanded unit cell in c). Part d) illustrates the four G_1 graphs that actually need to be considered.

Sutherland lattice in such a way that every dimer belongs to exactly one structure, the interactions that traverse the border between two structures can obviously be described as a number of type A and type B triangles as illustrated in figure 4.3 a). If the pinwheel structures are treated as "super-nodes" of a graph, a "super-bond" R can be defined as a set of type 1 and type 2 triangles or "Shastry bonds" between any two pinwheel structures. The question may arise why these triangular bonds are defined as the elementary link instead of simple two-site couplings. Recalling the discussion of the inter-dimer part of the Shastry-Sutherland Hamiltonian (2.4), we have seen that $H|\triangleright_{i,j,k}\rangle$ vanishes if the dimer (i,j) is in a singlet state; in other words, a description of the Shastry-Sutherland lattice in terms of triangular bonds already contains its specific geometric frustration in a natural way. Looking at the dimers that form the bases of the green and yellow triangular bonds in figure 4.1 and 4.2, we find that they belong to sites with a very high singlet density as illustrated in figure 3.1 and 3.2. The small triplet density at these sites corresponds to a small expansion parameter or fluctuation path and thus justifies the assumption of the real ground state of a crystal structure being close to the product state of the isolated structures discussed before.

Returning to the technical details of a graph expansion, we consider the simplest class of subgraphs G_0 of such an arrangement which obviously is the pinwheel structure itself (one node, no edges). A graph expansion up to order zero hence is the approximation of the ground state by a product state where the factors are the ground state wave functions of the constituent clusters. In the following illustrations, this energy is formally set to zero for the sake of simplicity, but has to be accounted for during the calculations.

The next class of subgraphs G_1 made of pinwheel structures consists of two nodes

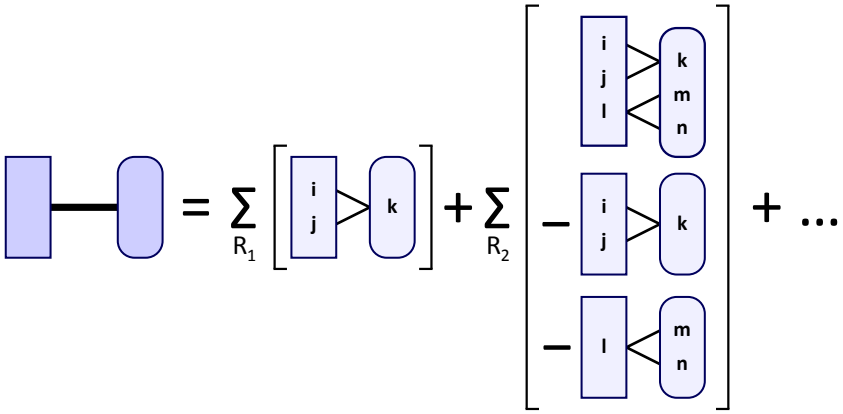

Figure 4.4.: "Inner" graph expansion of a single super-bond, only first and second order are shown. The set R_1 (R_2) contains all Shastry bonds (i,j,k) (pairs of Shastry bonds (i,j,k), (l,m,n)) that form the super-bond.

connected by one super-bond. For clarification, consider a regular lattice of pinwheel structures such as that in figure 4.3 b). It consists of two different kinds of super-nodes, denoted by a circle and a square, respectively, which are connected by four different kinds of super-bonds visualized by different line styles. It is clear that the determination of the contribution of G_1 to the ground-state energy per site (or per unit cell) only requires the analysis of the four graphs depicted in part d) since a multiplication by the number of ways a G_1 class subgraph can be arranged on the lattice cancels out with the division by the number of unit cells.

Figure 4.4 illustrates the further handling of such a G_1 subgraph. Basically, a second "inner" graph expansion within the first calculation is performed. This time, every Shastry bond constitutes an edge, and all connected graphs with at least one edge only differ in the number of edges between their two nodes. The zero order expansion (one node, no edges) yields the unperturbed ground-state energies as in the previous paragraph and is not depicted in figure 4.4. The first non-trivial contribution is caused by all graphs consisting of the two pinwheel structures connected by a single Shastry bond, which is illustrated by the first summation in figure 4.4. The next (second order) contribution is associated with all graphs consisting of the two pinwheel structures connected by two Shastry bonds minus the contribution of the two subgraphs it contains (second summation) and so on.

Though this formulation in terms of a nested graph expansion is a very useful way of ordering the different corrections to the ground-state energy, the question posed at the beginning of this chapter has not yet been fully answered: Can these expansions be truncated at some point without losing too much information, i.e. will the contributions finally become negligibly small? The expansion of the effective Hamiltonian of the Shastry-Sutherland model in terms of J'/J that was described briefly in chapter 2 might serve as a first starting point. As the first order terms only consist of nearest-neighbour interactions (see appendix A.1), they are already fully contained in the first summand of figure 4.4 (together with nearest-neighbour terms

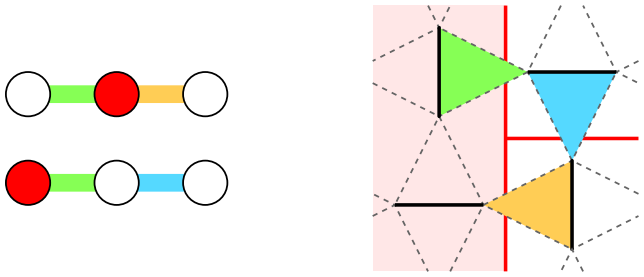

Figure 4.5.: Two examples of potential $(J'/J)^2$ fluctuations that are neglected when using an outer graph expansion of order one, independent of the degree of the inner expansion. The left part illustrates the situation on the level of graphs while the right parts shows the involved Shastry bonds.

of up to infinite order). The second order contributions are more complicated as they contain several correlated-hopping processes involving three dimers. Though some of them are included when the inner expansion is advanced to second order, a situation as illustrated in figure 4.5 is problematic, as it needs the outer expansion to advance to order two (three pinwheel structures connected by a number of super-bonds). When the clusters constituting the super-sites are comparably large, effects as in figure 4.5 should be small. In the case of a super-site consisting of a single dimer, however, neglecting this fact leads to obviously erroneous results. To sum up, it is not constructive to advance the "inner" graph expansion up to arbitrarily high order while leaving the situation illustrated in figure 4.3 b) to d) unchanged.

If all the pitfalls caused by the synchronization between outer and inner graph expansion are avoided, there is still one problem left, namely the computation of the summands in figure 4.4 which is discussed in the next section.

4.2.2. Hilbert Space Truncation

As the entire spectrum of the isolated structures is not available, Rayleigh Schrödinger perturbation theory is only applicable up to order one which basically yields the product of the local magnetizations

$$E_R^{(1)} = \langle 0|V|0\rangle = J' \sum_{\triangleright(i,j,k)\in R} \langle S_i^z + S_j^z\rangle_A \langle S_k^z\rangle_B + J' \sum_{\triangleleft(i,j,k)\in R} \langle S_i^z\rangle_A \langle S_j^z + S_k^z\rangle_B .$$

This motivates the employment of an approximation technique developed by Kris Coester [1]. Basically, the projection of the total Hamiltonian onto a small subspace is diagonalized, and its lowest eigenvalue can be used as an approximation of the actual ground state when this subspace has been well chosen.

To evaluate one of the summands illustrated in the center part of figure 4.4, the Hamilton operator

$$H = H_0 + V_{ijk} := H_A \otimes \mathbb{1}_B + \mathbb{1}_A \otimes H_B + J' \left(\boldsymbol{S}_i + \boldsymbol{S}_j\right) \boldsymbol{S}_k$$

has to be diagonalized within the product space of the two structures A and B which is numerically impossible. Instead, a subspace

$$\begin{aligned}\mathcal{S} &:= \text{span}\left\{|0\rangle, V_{ijk}|0\rangle\right\} \\ &= \text{span}\left\{|0\rangle_A|0\rangle_B, \left(\boldsymbol{S}_i + \boldsymbol{S}_j\right)|0\rangle_A \boldsymbol{S}_k|0\rangle_B\right\} \\ &= \text{span}\left\{|0\rangle_A|0\rangle_B, \left(W_{+-} + W_{-+} + W_z\right)|0\rangle_A|0\rangle_B\right\}\end{aligned}$$

is created where the second basis vector has been split up into the sum of three product states

$$\begin{aligned}W_{+-}|0\rangle_A|0\rangle_B &:= \left(S_i^+ + S_j^+\right)|0\rangle_A S_k^-|0\rangle_B \\ W_{-+}|0\rangle_A|0\rangle_B &:= \left(S_i^- + S_j^-\right)|0\rangle_A S_k^+|0\rangle_B \\ W_z|0\rangle_A|0\rangle_B &:= 2\left(S_i^z + S_j^z\right)|0\rangle_A S_k^z|0\rangle_B .\end{aligned}$$

To compute the matrix elements of the projection of H onto $\mathcal{S}$, the second basis vector has to be orthonormalized with respect to $|0\rangle$ using the Gram-Schmidt process which adds a fourth summand. The lower eigenvalue of the resulting 2×2 matrix is then given by

$$\lambda_- = \langle H_A\rangle + \langle H_B\rangle + \Delta_{ijk} \tag{4.1}$$

where $\langle H_A\rangle$ and $\langle H_B\rangle$ are the ground-state energies of the structures A and B, respectively, and Δ_{ijk} denotes the approximative contribution of this graph consisting of two super-nodes and one Shastry bond (i,j,k). Note that the composition of λ_- as in equation (4.1) is the mathematical formulation of the strategy described at the beginning of the previous section: Only those contributions are attributed to a certain graph that are not present in any of its subgraphs, the only difference being that Δ_{ijk} is just an approximation of that contribution as the exact solution of the structure described by the graph under consideration is not available.

To obtain the corrections of a graph consisting of two super-nodes and two Shastry bonds as illustrated in the second part of figure 4.4, the Hamiltonian

$$H = H_0 + V_{ijk} + V_{lmn} := H_A \otimes \mathbb{1}_B + \mathbb{1}_A \otimes H_B + J'\left(\boldsymbol{S}_i + \boldsymbol{S}_j\right)\boldsymbol{S}_k + J'\left(\boldsymbol{S}_l + \boldsymbol{S}_m\right)\boldsymbol{S}_n \tag{4.2}$$

is projected onto the subspace

$$\mathcal{T} := \text{span}\left\{|0\rangle, V_{ijk}|0\rangle, V_{lmn}|0\rangle\right\}$$

which results in a 3×3 matrix whose lowest eigenvalue can be written as

$$\mu_- = \langle H_A\rangle + \langle H_B\rangle + \Delta_{ijk} + \Delta_{lmn} + \Xi_{ijklmn}$$

where Ξ is the approximative contribution of this graph. Note that the operator V_{lmn} in equation (4.2) has to be adjusted to $\boldsymbol{S}_l\left(\boldsymbol{S}_m + \boldsymbol{S}_n\right)$ if the two Shastry bonds under consideration are of different types (i.e. $\triangleright$, $\triangleleft$).

Though physically plausible, the quality of these approximations is hard to estimate in full generality. At least for the case of a single Shastry bond where an effective 2×2 matrix is considered, some mathematical backup is given by the following

Theorem. *Let H_0 and V be two Hermitian operators on a finite-dimensional Hilbert space and $|0\rangle, \ldots, |n\rangle$ denote the eigenstates of H_0 with the corresponding eigenvalues $E_0, \ldots, E_n$. Let $H := H_0 + xV$ be the perturbed Hamilton operator with ground-state energy E_0' and its Rayleigh Schrödinger approximation*

$$E_0' = E_R^{(0)} + E_R^{(1)} x + + E_R^{(2)} x^2 + O(x^3).$$

The lower eigenvalue of H, projected onto span $\{|0\rangle, V|0\rangle\}$*, is then given by*

$$\epsilon_0' = \epsilon^{(0)} + \epsilon^{(1)} x + \epsilon^{(2)} x^2 + O(x^3)$$

with $\epsilon^{(0)} = E_R^{(0)}$, $\epsilon^{(1)} = E_R^{(1)}$ and

$$\left| \frac{\epsilon^{(2)} - E_R^{(2)}}{E_R^{(2)}} \right| \leq \frac{\tilde{E} - E_1}{\tilde{E} - E_0} \tag{4.3}$$

where

$$\tilde{E} := \frac{\sum_{k=1}^{n} E_k |\langle 0|V|k\rangle|^2}{\sum_{k=1}^{n} |\langle 0|V|k\rangle|^2}.$$

A proof of this theorem is given in appendix A.4. Basically, the approximation is exact up to first order using Rayleigh Schrödinger perturbation theory, and the approximation of the second order is best when the gap $E_1 - E_0$ is large and the perturbation V is unlikely to map the ground state to excitations with a high energy. Under the exemplary assumptions of a gap as it is observed in the smallest pinwheel structure, an otherwise equidistant spectrum E_k and $|\langle 0|V|k\rangle| \propto k^{-1}$ the estimate (4.3) yields a maximum relative error of about 3%.

4.3. Results

Table 4.1 summarizes the ground-state energies obtained for the crystal structures associated with the $1/5, 1/6, 1/8$ and $2/15$ plateaus using different approximations, together with the corresponding results by Corboz and Mila. The analysis of the two crystal structures which contain the largest cluster using first order graph expansion already necessitates the use of MPI parallelization; a second order expansion of these structures would require disproportionately greater efforts while unlikely to yield important corrections so the expansion was not carried further at this point.

Some tendencies are clearly visible from table 4.1: First, the approximations successively approach the results obtained with iPEPS which confirms the general applicability of the non-perturbative ansatz presented in this thesis. Second, the approximations are best for those unit cells made of large structures which supports

Crystal	Product State	RS 1	GE 1 + 1	GE 1 + 2	iPEPS [2]
1/5	−0.324 82	−0.322 61	−0.326 22	−0.326 16	−0.326 84
1/6	−0.334 44	−0.333 20	−0.335 90	−0.335 91	−0.336 76
2/15	−0.345 19	−0.344 41	−0.346 29	–	−0.346 09
1/8	−0.347 75	−0.347 47	−0.348 05	–	−0.348 12

Table 4.1.: Ground state energies per spin of the crystal structures presented in figure 3.1 and 3.2 obtained with different approximations. RS 1 is short for Rayleigh Schrödinger perturbation theory up to order one, "GE a + b" denotes a graph expansion of order a with respect to the super-bonds and order b with respect to the Shastry bonds (see section 4.2.1).

the interpretation of the triplet density at the peripheral sites as a small expansion parameter. Third, the second order expansion of the ground-state energies of the 1/5 and 1/6 configuration does not yield significant corrections while the approximation remains suboptimal. This suggests the conclusion that processes involving three (or more) super-sites as illustrated in figure 4.5 might considerably contribute to the ground-state energies of the crystals with small unit cells.

In figure 4.6, the plateau energies are plotted as a function of the external magnetic field using equation (2.3). As the intersection of any two of these lines is highly susceptible to small deviations in the axis intercept (i.e. the ground-state energy), the low energy of the 2/15 crystal in combination with the high energy of the 1/6 crystal leads to a series of magnetization plateaus which is no longer consistent with iPEPS although the results are energetically close to each other.

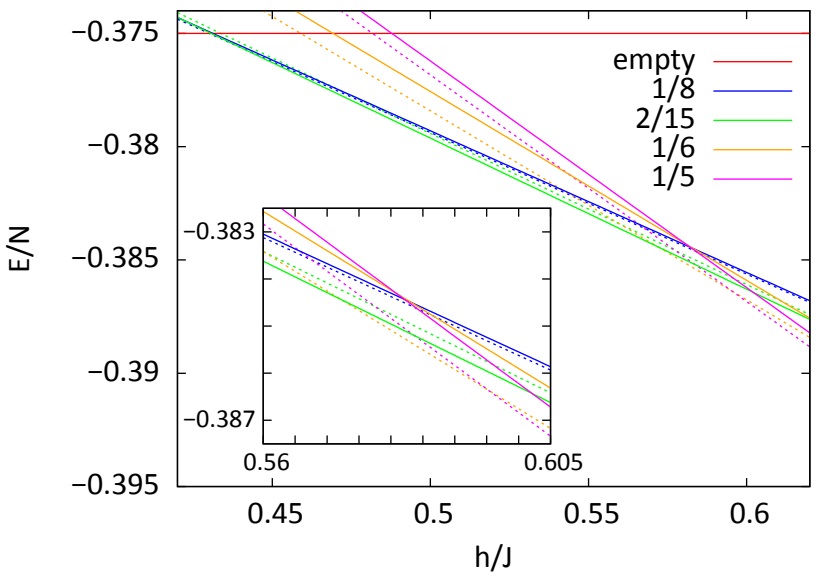

Figure 4.6.: Ground-state energies of the four crystals as a function of the external magnetic field. Dashed lines denote the results obtained with iPEPS.

5. Summary and Outlook

We began with the discussion of the characteristic properties of the Shastry-Sutherland model in the limiting cases of large and weak inter-dimer coupling. The product state of singlets was shown to remain an exact eigenstate for arbitrary values of J', and the conservation of S^z_{tot} was used to restrict all further analysis to the case without any external magnetic field. By solving the Shastry-Sutherland model on a number of finite clusters in the $S^z_{\text{tot}} = 2$ subspace using ED techniques, the bound states of triplets discovered by Corboz and Mila were reproduced and shown to have s-wave symmetry. The singlet and triplet densities were calculated on these structures and used as a motivation of an expansion technique to assemble crystals of these bound states.

Starting from the pure product state, first order perturbation theory as well as first and second order graph expansions were employed to obtain successive approximations of the "true" ground-state energies computed by Corboz and Mila. A truncation scheme was presented to obtain estimates of the ground-state energies of clusters connected by a number of Shastry bonds which were argued to constitute the elementary links on the frustrated Shastry-Sutherland lattice. Considering the $1/8$ and the $2/15$ plateaus, the results of these calculations are in excellent ($\leq 2 \cdot 10^{-4}$) agreement with iPEPS whereas the crystal structures associated with the $1/5$ and $1/6$ plateaus (small unit cells) are energetically overestimated ($\approx 10^{-3}$) even though the inner graph expansion shows convergent behaviour. It was suggested that one possible reason might be the neglect of contributions caused by fluctuations spanning three ore more clusters (super-sites) which would affect the small unit cells most.

If these further corrections turn out to be sufficient, the non-perturbative method presented in this thesis will be suited to make predictions as to the dependence of the magnetization plateaus of the coupling parameter J' at comparably low numerical costs. Regarding the substance $SrCu_2(BO_3)_2$, J' can be varied within a small range by applying external pressure so these predictions could actually be verified experimentally.

As the ED techniques presented in chapter 3 are not limited to the pure Shastry-Sutherland model, the influence of asymmetric Dzyaloshinskii-Moriya interactions as they are present in $SrCu_2(BO_3)_2$ [14, 3] could also be included in further analyses. As they, however, do not conserve the z component of the total spin in general, the respective diagonalizations as well as the subsequent expansion techniques will require additional numerical efforts.

A. Appendix

A.1. Effective Hamiltonian of the Shastry-Sutherland Model

The following strong-coupling expansion of the effective Hamiltonian of the Shastry-Sutherland model up to order two in J'/J is taken from the work of Momoi [15]; only those processes contained in the subspace with maximum S^z_{tot} are considered. Every dimer is associated with a site i on an effective square lattice with the canonical unit vectors $\boldsymbol{e}_1$ and $\boldsymbol{e}_2$. The sublattice A (B) only contains the horizontal (vertical) dimers, NN abbreviates a sum over the next neighbours.

$$
\begin{aligned}
H &= H_0 + H_1 + H_2 + \dots \\
H_0 &= (J-h)\sum_i n_i \\
H_1 &= \frac{J'}{2}\sum_{NN} n_i n_j \\
H_2 &= -\frac{J'^2}{J}\sum_i n_i + \frac{J'^2}{2J}\sum_{NN} n_i n_j + \frac{J'^2}{4J}\sum_{i\in A}\{2n_{i+\boldsymbol{e}1}\,(1-n_i)\,n_{i-\boldsymbol{e}1} \\
&\quad + \left(b^\dagger_{i+\boldsymbol{e}2} b_{i-\boldsymbol{e}2} + \text{h.c.}\right) n_i + \left(b^\dagger_i b_{i+\boldsymbol{e}2} - b^\dagger_i b_{i-\boldsymbol{e}2} + \text{h.c.}\right) \times (n_{i-\boldsymbol{e}1} - n_{i+\boldsymbol{e}1})\} \\
&\quad + \frac{J'^2}{4J}\sum_{i\in B}\{\boldsymbol{e}_1 \leftrightarrow \boldsymbol{e}_2\}
\end{aligned}
$$

A.2. Routines Used for Exact Diagonalization

Algorithm 1.1 Creation of a mapping $J = J_a + J_b$ for a given S^z_{tot}.

Require: S^z_{tot}
Ensure: J_a, J_b
$c \leftarrow N/2 + S^z_{\text{tot}}$ ▷ corresponding number of up spins
ctrA $\leftarrow 0$
for $I_a = 0, 1, 2, \dots, 2^{N/2} - 1$ **do**
    ctrB $\leftarrow 0$
    for all I_b such that Ham $(2^{N/2} I_a + I_b) = c$ **do**
        add $I = 2^{N/2} I_a + I_b$ to the list of states
        ctrB $\leftarrow$ ctrB + 1
        $J_a(I_a) \leftarrow$ ctrA
        $J_b(I_b) \leftarrow$ ctrB
    end for
    ctrA $\leftarrow$ ctrA + ctrB
end for

Algorithm 1.2 Basic Lanczos algorithm to approximate the lowest eigenvalue of A.

Require: tolerance ϵ
Ensure: eigenpair approximation $\mu, \boldsymbol{u}$
create random starting vector $\boldsymbol{r}$
$\beta_0 \leftarrow \|\boldsymbol{r}\|_2$
$\boldsymbol{v}_0 \leftarrow 0$
$j \leftarrow 0$
repeat
  $j \leftarrow j + 1$
  $\boldsymbol{v}_j \leftarrow \boldsymbol{r}/\beta_{j-1}$
  $\boldsymbol{r} \leftarrow A\boldsymbol{v}_j$
  $\boldsymbol{r} \leftarrow \boldsymbol{r} - \beta_{j-1}\boldsymbol{v}_{j-1}$
  $\alpha_j \leftarrow \boldsymbol{v}_j \cdot \boldsymbol{r}$
  $\boldsymbol{r} \leftarrow \boldsymbol{r} - \alpha_j \boldsymbol{v}_j$
  optional reorthogonalization
  $\beta_j \leftarrow \|\boldsymbol{r}\|_2$
  $T_j \leftarrow \begin{pmatrix} \alpha_1 & \beta_1 & & & \\ \beta_1 & \alpha_2 & \beta_2 & & \\ & \ddots & \ddots & \ddots & \\ & & \ddots & \ddots & \beta_{n-1} \\ & & & \beta_{n-1} & \alpha_n \end{pmatrix}$
  $\lambda_j \leftarrow$lowest eigenvalue of T_j
  $\boldsymbol{s}^{(j)} \leftarrow$corresponding (normalized) eigenvector
  if $\left|\beta_j s_j^{(j)}\right| < \epsilon$ **then** mark the eigenvalue as converged
  end if
until convergence
$\mu \leftarrow \lambda_j$
restart algorithm to compute the eigenvector $\boldsymbol{u} = \begin{pmatrix} \boldsymbol{v}_1 & \boldsymbol{v}_2 & \dots & \boldsymbol{v}_j \end{pmatrix} \boldsymbol{s}^{(j)}$

A.3. Dimer-dimer Correlations

In this section the calculation of the correlation between a dimer k_1 and another dimer $k_2 \neq k_1$ is demonstrated. For the sake of simplicity, let $k_1 = 1$ and $k_2 = 2$; the other cases are treated analogously. Using the notation defined in section 3.2, $\mathcal{H}$ can be decomposed into a product of dimer spaces in the following way:

$$\mathcal{H} = \mathcal{D}_1 \otimes \mathcal{D}_2 \otimes \prod_{k=3}^{N/2} \mathcal{D}_k$$

Using the projection operator

$$Q(|\psi\rangle) : \mathcal{H} \to \mathcal{U} \qquad |\psi\rangle \in \text{span}\,\{|\uparrow\uparrow\uparrow\uparrow\rangle, \dots, |\downarrow\downarrow\downarrow\downarrow\rangle\} = \mathcal{D}_1 \otimes \mathcal{D}_2$$

onto the subspace

$$\mathcal{U} = \text{span}\,|\psi\rangle \otimes \prod_{k=3}^{N/2} \mathcal{D}_k,$$

the 16 dimer-dimer correlations $\langle \alpha_1 \beta_2 \rangle$ are defined as

$$\langle \alpha_1 \beta_2 \rangle := \langle 0 | D \left(|\alpha\rangle_1 |\beta\rangle_2 \right) |0\rangle$$

where

$$\alpha, \beta \in \left\{ s^0, t^+, t^0, t^- \right\}.$$

Again, for practical computations it is more convenient to write for all i

$$c_i |b_i\rangle = c_i^{|d_i^{(1)} d_i^{(2)}\rangle} |d_i^{(1)} d_i^{(2)} e_i\rangle \quad \text{where} \quad |d_i^{(1)} d_i^{(2)}\rangle \in \mathcal{D}_1 \otimes \mathcal{D}_2,$$

which finally yields

$$\begin{aligned}
\langle s_1^0 s_2^0 \rangle &= \frac{1}{4} \sum_{\substack{e_i \\ |\uparrow\downarrow\uparrow e_i\rangle \in E_2}} \left| c_i^{|\uparrow\downarrow\uparrow\downarrow\rangle} - c_i^{|\uparrow\downarrow\downarrow\uparrow\rangle} - c_i^{|\downarrow\uparrow\uparrow\downarrow\rangle} + c_i^{|\downarrow\uparrow\downarrow\uparrow\rangle} \right|^2 \\
\langle s_1^0 t_2^- \rangle &= \frac{1}{2} \sum_{\substack{e_i \\ |\uparrow\downarrow\downarrow e_i\rangle \in E_2}} \left| c_i^{|\uparrow\downarrow\downarrow\downarrow\rangle} - c_i^{|\downarrow\uparrow\downarrow\downarrow\rangle} \right|^2 \\
\langle s_1^0 t_2^0 \rangle &= \frac{1}{4} \sum_{\substack{e_i \\ |\uparrow\downarrow\uparrow e_i\rangle \in E_2}} \left| c_i^{|\uparrow\downarrow\uparrow\downarrow\rangle} + c_i^{|\uparrow\downarrow\downarrow\uparrow\rangle} - c_i^{|\downarrow\uparrow\uparrow\downarrow\rangle} - c_i^{|\downarrow\uparrow\downarrow\uparrow\rangle} \right|^2 \\
\langle s_1^0 t_2^+ \rangle &= \frac{1}{2} \sum_{\substack{e_i \\ |\uparrow\downarrow\uparrow\uparrow e_i\rangle \in E_2}} \left| c_i^{|\uparrow\downarrow\uparrow\uparrow\rangle} - c_i^{|\downarrow\uparrow\uparrow\uparrow\rangle} \right|^2 \\
\langle t_1^- t_2^- \rangle &= \sum_{\substack{e_i \\ |\downarrow\downarrow\downarrow\downarrow e_i\rangle \in E_2}} \left| c_i^{|\downarrow\downarrow\downarrow\downarrow\rangle} \right|^2 \\
\langle t_1^- t_2^0 \rangle &= \frac{1}{2} \sum_{\substack{e_i \\ |\downarrow\downarrow\uparrow\downarrow e_i\rangle \in E_2}} \left| c_i^{|\downarrow\downarrow\uparrow\downarrow\rangle} + c_i^{|\downarrow\downarrow\downarrow\uparrow\rangle} \right|^2 \\
\langle t_1^- t_2^+ \rangle &= \sum_{\substack{e_i \\ |\downarrow\downarrow\uparrow\uparrow e_i\rangle \in E_2}} \left| c_i^{|\downarrow\downarrow\uparrow\uparrow\rangle} \right|^2 \\
\langle t_1^0 t_2^0 \rangle &= \frac{1}{4} \sum_{\substack{e_i \\ |\uparrow\downarrow\uparrow\downarrow e_i\rangle \in E_2}} \left| c_i^{|\uparrow\downarrow\uparrow\downarrow\rangle} + c_i^{|\uparrow\downarrow\downarrow\uparrow\rangle} + c_i^{|\downarrow\uparrow\uparrow\downarrow\rangle} + c_i^{|\downarrow\uparrow\downarrow\uparrow\rangle} \right|^2 \\
\langle t_1^0 t_2^+ \rangle &= \frac{1}{2} \sum_{\substack{e_i \\ |\uparrow\downarrow\uparrow\uparrow e_i\rangle \in E_2}} \left| c_i^{|\uparrow\downarrow\uparrow\uparrow\rangle} + c_i^{|\downarrow\uparrow\uparrow\uparrow\rangle} \right|^2 \\
\langle t_1^+ t_2^+ \rangle &= \sum_{\substack{e_i \\ |\uparrow\uparrow\uparrow\uparrow e_i\rangle \in E_2}} \left| c_i^{|\uparrow\uparrow\uparrow\uparrow\rangle} \right|^2 .
\end{aligned}$$

By swapping $\langle \alpha_1 \beta_2 \rangle \to \langle \alpha_2 \beta_1 \rangle$ and $c_i |d_i^{(1)} d_i^{(2)}\rangle \to c_i |d_i^{(2)} d_i^{(1)}\rangle$, the remaining 8 combinations can be obtained.

A.4. Proof of the Truncation Theorem

Let H_0 and V be two Hermitian operators on a finite-dimensional Hilbert space and $|0\rangle, \ldots, |n\rangle$ denote the eigenstates of H_0 with the corresponding eigenvalues $E_0 \leq E_1 \leq \cdots \leq E_n$. Let $H := H_0 + xV$ be the perturbed Hamilton operator with ground-state energy E_0' and its Rayleigh Schrödinger approximation

$$E_0' = E_R^{(0)} + E_R^{(1)} x + E_R^{(2)} x^2 + O(x^3).$$

To obtain a matrix representation of H, projected onto span $\{|0\rangle, V|0\rangle\}$, we choose the orthonormal basis $\{|0\rangle, |v\rangle\}$ where

$$|v\rangle := \frac{1}{N} \sum_{k=1}^{n} |k\rangle \langle k|V|0\rangle \qquad N := \sqrt{\sum_{k=1}^{n} |\langle k|V|0\rangle|^2}.$$

The (real) matrix representation of $H = H_0 + xV$ in the chosen subspace can then be written in the form

$$\begin{pmatrix} A & C \\ C & B \end{pmatrix}$$

where

$$\begin{aligned} A &= E_0 + xV_{00} \\ B &= \frac{1}{N^2} \left(\sum_{k=1}^{n} |V_{k0}|^2 E_k + x \sum_{k,l=1}^{n} V_{0l} V_{k0} V_{lk} \right) \\ C &= \frac{x}{N} \sum_{k=1}^{n} |V_{k0}|^2 \end{aligned}$$

with the abbreviation $V_{ij} := \langle i|V|j\rangle$. The lower eigenvalue of this matrix is expanded in a Taylor series up to order two in x:

$$\begin{aligned} \lambda_- &= \frac{A+B}{2} - \sqrt{\left(\frac{A-B}{2}\right)^2 + C^2} \\ &= E_0 + xV_{00} + x^2 \sum_{k=1}^{n} \frac{|V_{k0}|^2}{E_0 - \tilde{E}} + O\left(x^3\right) \\ &= \epsilon^{(0)} + x\epsilon^{(1)} + x^2\epsilon^{(2)} + O\left(x^3\right) \end{aligned} \tag{A.1}$$

where we introduced the abbreviation

$$\tilde{E} := \frac{\sum_{k=1}^{n} |V_{k0}|^2 E_k}{\sum_{k=1}^{n} |V_{k0}|^2} =: \sum_{k=1}^{N} \rho_k E_k \in [E_1, E_n] \tag{A.2}$$

which can be interpreted as a special energetic average of the excitations of the ground states caused by V with the respective probability distribution ρ_k. Note that equation (A.1) only holds if $E_0 \leq \tilde{E}$ which is no constriction because of equa-

tion (A.2).

Using the definitions of the first three terms of the Rayleigh Schrödinger perturbation series we obtain

$$\begin{aligned} E_R^{(0)} &:= E_0 \overset{(A.1)}{=} \epsilon^{(0)} \\ E_R^{(1)} &:= V_{00} \overset{(A.1)}{=} \epsilon^{(1)} \\ E_R^{(2)} &:= \sum_{k=1}^{n} \frac{|V_{k0}|^2}{E_0 - E_k}, \end{aligned}$$

so exact equality to the expansion (A.1) obviously holds up to order one. Although the second order terms have the same sign, they differ in the weights that are applied to the transition amplitudes $|V_{k0}|^2$. In Rayleigh Schrödinger perturbation theory, each amplitude is weighted individually by $(E_k - E_0)^{-1}$ while all the amplitudes are weighted equally by $(\tilde{E} - E_0)^{-1}$ in equation (A.1).

To finally prove the error estimate, let $m \in \{1, \dots, n-1\}$ such that $\tilde{E} \in [E_m, E_{m+1}]$. The relative difference between the second order correction in the Rayleigh Schrödinger expansion and $\epsilon^{(2)}$ fulfils

$$\begin{aligned} \left| \frac{\epsilon^{(2)} - E_R^{(2)}}{E_R^{(2)}} \right| &= \left| 1 - \frac{\sum_{k=1}^{n} \frac{|V_{k0}|^2}{\tilde{E}-E_0}}{\sum_{k=1}^{n} \frac{|V_{k0}|^2}{E_k-E_0}} \right| \\ &= \left| 1 - \frac{\sum_{k=1}^{n} \frac{|V_{k0}|^2}{\tilde{E}-E_0}}{\sum_{k=1}^{m} \frac{|V_{k0}|^2}{E_k-E_0} + \sum_{k=m+1}^{n} \frac{|V_{k0}|^2}{E_k-E_0}} \right| \\ &\leq \left| 1 - \frac{\sum_{k=1}^{n} \frac{|V_{k0}|^2}{\tilde{E}-E_0}}{\sum_{k=1}^{m} \frac{|V_{k0}|^2}{E_1-E_0} + \sum_{k=m+1}^{n} \frac{|V_{k0}|^2}{\tilde{E}-E_0}} \right| \\ &= \left| 1 - \left(\frac{\tilde{E} - E_0}{E_1 - E_0} \underbrace{\frac{\sum_{k=1}^{m} |V_{k0}|^2}{\sum_{k=1}^{n} |V_{k0}|^2}}_{\leq 1} + \underbrace{\frac{\sum_{k=m+1}^{n} |V_{k0}|^2}{\sum_{k=1}^{n} |V_{k0}|^2}}_{\leq 1} \right)^{-1} \right| \\ &\leq \left| 1 - \frac{E_1 - E_0}{\tilde{E} - E_0} \right| \\ &= \frac{\tilde{E} - E_1}{\tilde{E} - E_0}. \end{aligned}$$

□

Bibliography

[1] K. Coester. Personal communication.

[2] P. Corboz. Personal communication.

[3] P. Corboz and F. Mila. "Crystals of Bound States in the Magnetization Plateaus of the Shastry-Sutherland Model". In: *Physical Review Letters* 112.14, 147203 (Apr. 2014), p. 147203. DOI: 10.1103/PhysRevLett.112.147203.

[4] P. Corboz and F. Mila. "Tensor network study of the Shastry-Sutherland model in zero magnetic field". In: *Phys. Rev. B* 87 (11 2013), p. 115144. DOI: 10.1103/PhysRevB.87.115144.

[5] E. R. Davidson. "The iterative calculation of a few of the lowest eigenvalues and corresponding eigenvectors of large real-symmetric matrices". In: *Journal of Computational Physics* 17.1 (1975), pp. 87 –94. ISSN: 0021-9991. DOI: 10.1016/0021-9991(75)90065-0.

[6] J. Dorier, K. P. Schmidt, and F. Mila. "Theory of Magnetization Plateaux in the Shastry-Sutherland Model". In: *Phys. Rev. Lett.* 101 (25 2008), p. 250402. DOI: 10.1103/PhysRevLett.101.250402.

[7] G. R. Foltin, S. R. Manmana, and K. P. Schmidt. "Exotic magnetisation plateaus in a quasi-2D Shastry-Sutherland model". In: *ArXiv e-prints* (May 2014). arXiv: 1405.3260 [cond-mat.str-el].

[8] K. Kodama et al. "Magnetic Superstructure in the Two-Dimensional Quantum Antiferromagnet SrCu2(BO3)2". In: *Science* 298.5592 (2002), pp. 395–399. DOI: 10.1126/science.1075045.

[9] C. Lanczos. "An Iteration Method for the Solution of the Eigenvalue Problem of Linear Differential and Integral Operators". In: *Journal of Research of the National Bureau of Standards* 45 (4 1950), pp. 255–282.

[10] H. Q. Lin. "Exact diagonalization of quantum-spin models". In: *Phys. Rev. B* 42 (10 1990), pp. 6561–6567. DOI: 10.1103/PhysRevB.42.6561.

[11] J. Lou et al. "Study of the Shastry Sutherland Model Using Multi-scale Entanglement Renormalization Ansatz". In: *ArXiv e-prints* (Dec. 2012). arXiv: 1212.1999 [cond-mat.str-el].

[12] A. Lüscher and A. Läuchli. "Exact diagonalization study of the antiferromagnetic spin-$\frac{1}{2}$ Heisenberg model on the square lattice in a magnetic field". In: *Phys. Rev. B* 79 (19 2009), p. 195102. DOI: 10.1103/PhysRevB.79.195102.

[13] Y. H. Matsuda et al. "Magnetization of $SrCu_2(BO_3)_2$ in Ultrahigh Magnetic Fields up to 118 T". In: *Physical Review Letters* 111.13, 137204 (Sept. 2013), p. 137204. DOI: 10.1103/PhysRevLett.111.137204.

[14] V. V. Mazurenko et al. "First-principles investigation of symmetric and antisymmetric exchange interactions of $SrCu_2(BO_3)_2$". In: *Phys. Rev. B* 78 (19 2008), p. 195110. DOI: 10.1103/PhysRevB.78.195110.

[15] T. Momoi and K. Totsuka. "Magnetization plateaus of the Shastry-Sutherland model for $SrCu_2(BO_3)_2$: Spin-density wave, supersolid, and bound states". In: *Phys. Rev. B* 62 (22 2000), pp. 15067–15078. DOI: 10.1103/PhysRevB.62.15067.

[16] M. Nemec, G. R. Foltin, and K. P. Schmidt. "Microscopic mechanism for the 1/8 magnetization plateau in $SrCu_2(BO_3)_2$". In: *Phys. Rev. B* 86 (17 2012), p. 174425. DOI: 10.1103/PhysRevB.86.174425.

[17] B. N. Parlett. *The symmetric eigenvalue problem*. Prentice-Hall series in computational mathematics. Englewood Cliffs, NJ: Prentice-Hall, 1980. ISBN: 0-13-880047-2.

[18] K. P. Schmidt and G. S. Uhrig. "Excitations in One-Dimensional $S = \frac{1}{2}$ Quantum Antiferromagnets". In: *Phys. Rev. Lett.* 90 (22 2003), p. 227204. DOI: 10.1103/PhysRevLett.90.227204.

[19] B. S. Shastry and B. Sutherland. "Exact ground state of a quantum mechanical antiferromagnet". In: *Physica B+C* 108.1–3 (1981), pp. 1069 –1070. ISSN: 0378-4363. DOI: 10.1016/0378-4363(81)90838-X.

[20] R. W. Smith and D. A. Keszler. "Synthesis, structure, and properties of the orthoborate $SrCu_2(BO_3)_2$". In: *Journal of Solid State Chemistry* 93.2 (1991), pp. 430 –435. ISSN: 0022-4596. DOI: 10.1016/0022-4596(91)90316-A.

[21] M. Takigawa et al. "Incomplete Devil's Staircase in the Magnetization Curve of $SrCu_2(BO_3)_2$". In: *Physical Review Letters* 110.6, 067210 (Feb. 2013), p. 067210. DOI: 10.1103/PhysRevLett.110.067210.

Danksagung

Mein besonderer Dank gilt meinen Betreuern Dr. Kai Schmidt, Kris Coester und Michael Powalski, die es mir ermöglicht haben, mit dieser Arbeit Einblicke in ein aktuelles Forschungsgebiet der Festkörpertheorie zu gewinnen, und mich mit vielen hilfreichen und geduldigen Diskussionen unterstützt haben. Herrn Prof. Dr. Götz Uhrig danke ich für die Übernahme des Zweitgutachtens.

Ich bedanke mich bei Herrn Dr. Carsten Raas für die schnelle und unkomplizierte Unterstützung in der Bedienung des PhiDo HPC Clusters, auf dem die Berechnungen in dieser Arbeit durchgeführt wurden.

Abschließend möchte ich Dr. Philippe Corboz und Prof. Frédéric Mila danken für die Übersendung ihrer numerischen Daten.

Eidesstattliche Versicherung

Ich versichere hiermit an Eides statt, dass ich die vorliegende Bachelorarbeit mit dem Titel „Non-perturbative Analysis of Crystals Formed by Bound Triplet States on the Shastry-Sutherland Lattice“ selbständig und ohne unzulässige fremde Hilfe erbracht habe. Ich habe keine anderen als die angegebenen Quellen und Hilfsmittel benutzt sowie wörtliche und sinngemäße Zitate kenntlich gemacht. Die Arbeit hat in gleicher oder ähnlicher Form noch keiner Prüfungsbehörde vorgelegen.

Ort, Datum | Unterschrift

Belehrung

Wer vorsätzlich gegen eine die Täuschung über Prüfungsleistungen betreffende Regelung einer Hochschulprüfungsordnung verstößt, handelt ordnungswidrig. Die Ordnungswidrigkeit kann mit einer Geldbuße von bis zu 50 000 € geahndet werden. Zuständige Verwaltungsbehörde für die Verfolgung und Ahndung von Ordnungswidrigkeiten ist der Kanzler bzw. die Kanzlerin der Technischen Universität Dortmund. Im Falle eines mehrfachen oder sonstigen schwerwiegenden Täuschungsversuches kann der Prüfling zudem exmatrikuliert werden (§ 63 Abs. 5 Hochschulgesetz - HG -).

Die Abgabe einer falschen Versicherung an Eides statt wird mit Freiheitsstrafe bis zu 3 Jahren oder mit Geldstrafe bestraft.

Die Technische Universität Dortmund wird ggf. elektronische Vergleichswerkzeuge (wie z.B. die Software „turnitin“) zur Überprüfung von Ordnungswidrigkeiten in Prüfungsverfahren nutzen.

Die oben stehende Belehrung habe ich zur Kenntnis genommen.

Ort, Datum | Unterschrift